PCCP

Accepted Manuscript

ROYAL SOCIETY OF CHEMISTRY

www.rsc.org/pccp

Cite this: DOI: 10.1039/c0xx00000x

www.rsc.org/xxxxxx

ARTICLE TYPE

A shuttle effect free lithium sulfur battery based on a hybrid electrolyte

Qingsong Wang,[a] Jun Jin,[a] Xiangwei Wu,[a] Guoqiang Ma,[a] Jianhua Yang[a] and Zhaoyin Wen,*[a]

Received (in XXX, XXX) Xth XXXXXXXXX 20XX, Accepted Xth XXXXXXXXX 20XX
DOI: 10.1039/b000000x

A room temperature hybrid electrolyte based lithium-sulfur cell was successfully cycled with an excellent coulombic efficiency of 100%. The initial discharge specific capacities of up to 1528 mAh g^{-1}, 1386 mAh g^{-1} and 1341 mAh g^{-1}, respectively, at C/20, C/5 and C/2 rates were realized and remained at 720 mAh g^{-1} after 40 cycles at C/5 rate.

The lithium sulfur (Li-S) system is proposed to be a promising candidate for energy storage batteries due to its high energy density. Its theoretical value (about 2600 Wh kg^{-1}) is drastically higher than that of state-of-the-art lithium ion batteries.[1, 2] In addition, elemental sulfur is of great abundance and environmental friendliness. Therefore, these appealing qualities enable Li-S batteries to attract worldwide attention and many breakthroughs have been achieved.[3-9] However, the practical application of the Li-S battery is still hindered by the capacity fading upon cycling, which can be mostly ascribed to the highly soluble intermediate polysulfide species in conventional liquid organic electrolyte solutions.[10-12] Generated at the cathode, these long-chain polysulfides with high mobility can migrate to the lithium anode where they are reduced to the insoluble Li_2S and the short-chain soluble polysulfides. Once become concentrated at the anode side, the short-chain polysulfides can diffuse back to the cathode side and will be re-oxidized into the original long-chain ones, thus creating a so-called shuttle effect. This shuttle effect results in the low utilization of active materials, poor coulombic efficiency and degradation of the lithium anode.[10, 13]

Recently, employing $LiNO_3$ salt as the electrolyte additive to form a stable protective film on the surface of lithium metal has been widely applied in liquid electrolyte Li-S batteries to suppress the shuttle effect [14-18]. The protective film prevents the direct contact between the polysulfides and lithium anode so that polysulfides can be protected from chemical and electrochemical reduction on the lithium anode[15, 19, 20]. However, the protective film is incapable of restraining lithium polysulfides from dissolving into the liquid electrolyte. Disadvantages are also brought in, though the presence of $LiNO_3$ in electrolyte can enhance the stability of the lithium anode and increase the cycle life of the batteries. The lithium anode progressively consumes $LiNO_3$ when the protective film grows unfailingly, and $LiNO_3$ may be reduced irreversibly on the cathode during the discharging process of cell.[17] Besides, the strong oxidative property of the $LiNO_3$ could also cause safety problems.[21] Therefore, using electrolyte additives can hardly settle the problems thoroughly and exploration of new prototype of Li-S cell would be an option to achieve excellent performances.

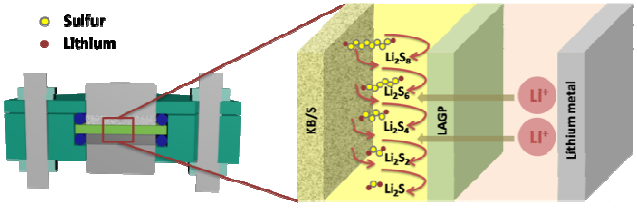

Figure 1. Schematic illustration of a HE Li-S cell.

The inorganic solid electrolyte, being of single-ion conduction, can prevent the solubility of the lithium polysulfides and hence turns out to be an ideal electrolyte materials for Li-S batteries.[22] In addition, inorganic solid electrolyte has the advantage of suppressing the formation the lithium dendrites for its mechanical strength[23]. Fabrication of all-solid-state Li-S batteries also attracts researchers' attention as an alternative approach to address the shuttle problem. Recently, Nagao *et al*. have reported a solid Li-S system developed by using thio-LISICON[24] and Agostini *et al*. have also reported a solid-state Li-S battery using a glass-type electrolyte with an operating temperature of 80°C[25]. However, major challenge exists in the electrode/electrolyte interface due to insufficient solid-solid contact resulting in a high interfacial resistance and thus the solid-state cell can only operate at a low current density. A possible way, reported by Hagen *et al*.[26], is to place a liquid organic solvent wetted polypropylene Celgard PP 2400 separator between the electrode and the solid electrolyte. Although operated successfully, only several cycles were achieved at a low rate C/100.

In this paper, we exploited an inorganic solid electrolyte, $Li_{1.5}Al_{0.5}Ge_{1.5}(PO_4)_3$ (LAGP) , as a separator for fabricating a hybrid electrolyte (HE) Li-S battery formed by a lithium metal anode and a Ketjen black-sulfur, KB/S, composite cathode. The NASICON-type structured LAGP electrolyte is an attractive candidate for solid electrolyte to develop lithium secondary battery for its favorable chemical stability against lithium and the wide electrochemical window up to 6 V (vs.Li/Li^+)[27]. The 1M $LiN(CF_3SO_2)_2$ in 1,3-dioxolane and 1,2-dimethoxyethane(1:1,v/v) (LiTFSI/DOL/DME) organic liquid electrolyte was used to connect the electrode and the solid electrolyte. The electrochemical performance of the HE Li-S cells at room temperature was investigated.

As schematically shown in Figure 1, the HE Li-S Cells were assembled by sandwiching the LAGP pellet between the lithium metal foil anode and the as-prepared KB/S cathode film. The cell sequence was placed in a predesigned Teflon container held by

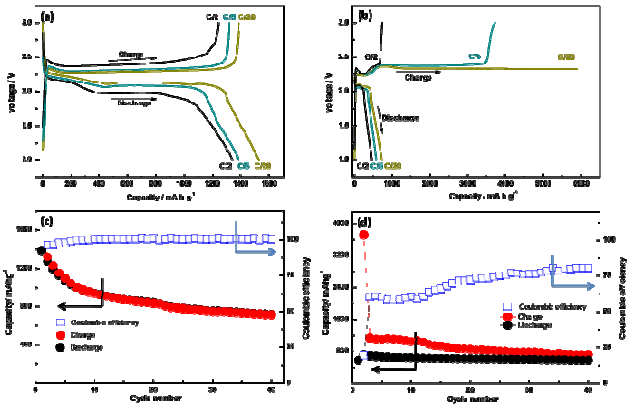

Figure 2. Voltage versus specific charge-discharge capacity profiles of initial galvanostatic cycles of (a) HE Li-S cells and (b) LE Li-S cells at C/2, C/5 and C/20 rates. Cycling performance and coulombic efficiency of (c) the HE Li-S cell and (d) the LE Li-S cell at C/5 rate. (Specific capacities are calculated based on sulfur mass.)

the screw clamp. 30 μl LiTFSI/DOL/DME was added into each of the catholyte and anolyte rooms. Stainless steel plates acted as current collectors and Teflon O-rings were used for sealing. For a comparison, CR2025 coin cells were also fabricated by using the Celgard 2400 microporous membrane as separator, and cells of this type are indicated in the text as liquid electrolyte Li-S cells (LE Li-S cells). All processes were performed in an argon filled glove box.

Figure S1 depicts the impendence spectra of the HE Li-S cell and the solid electrolyte LAGP. The cell impendence was measured before the cell undergoing further discharging-charging test. As shown, the Nyquist plot which is quite different from the typical one[28], composed of two partially overlapped semicircles and a straight slopping line. The depressed semicircle in the high frequency region (1 MHz-10 KHz) indicates the interphase contact resistance caused by the solid-liquid hybrid electrolyte interface. The other depressed semicircle in middle frequency region (10 KHz-10 Hz) reflects the charge-transfer resistance at the interface between the conductive agent and the electrolyte. The straight slopping line in the low frequency region (10 Hz-100 mHz) represents the diffusion impendence of Li-ion diffusion process. The left extrapolated intercept of the semicircle with the real axis in the high frequency region reflects the resistance of the solid electrolyte, whose value is very similar to the total resistance of the LAGP.

Figure 2a and Figure 2b shows voltage versus specific discharge capacity profiles of galvanostatic cycles at different rates. The open circuit voltage of the as-assembled HE Li-S cells was about 3.0 V. The charge-discharge curves represented a typical characterization of Li-S batteries with liquid electrolyte [5, 8, 29-31]. HE Li-S cells exhibit high initial discharge capacities (the theoretical specific capacity of sulfur, 1 C= 1675 mAh g^{-1}) of 1528 mAh g^{-1}_{sulfur}, 1386 mAh g^{-1}_{sulfur} and 1341 mAh g^{-1}_{sulfur}, respectively, at C/20, C/5 and C/2 rates. However, in LE Li-S cells, initial discharge capacities reach merely to 719 mAh g^{-1}_{sulfur}, 578 mAh g^{-1}_{sulfur}, 467 mAh g^{-1}_{sulfur}, respectively, at the same rates. Charge curves at lower current density become level at 2.3 V at which the concentration of long-chain polysulfides increases to a rather high degree[10, 32, 33]. The long-chain polysulfides, oxidation

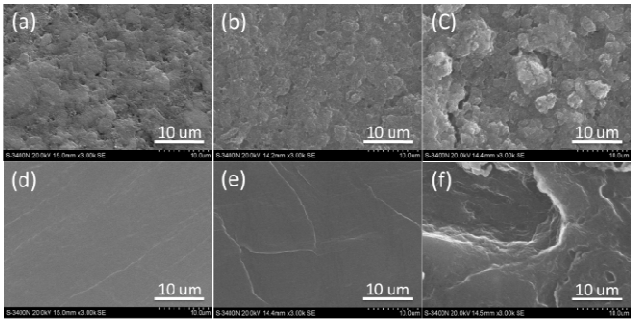

Figure 3. SEM images of sulfur cathodes and lithium anode at end of 10th charge cycle. (a) the initial cathode, (b) cathode cycled in HE cell, (c) cathode cycled in LE cell; (d) the fresh lithium anode, (e) the lithium anode cycled in HE cell, (f) the lithium anode cycled in LE cell.

products of short-chain polysulfides on the cathode, diffuse through the Celgard separator to the lithium electrode where they are reduced to regenerate short-chain polysulfides, thus leading to a severe shuttle effect. The short-chain polysulfides produced by the parasitic reaction diffuse back to cathode to generate the original long-chain polysulfides. This cyclic process goes on continually leading to the voltage leveling of the charge curve.[33] At higher charge current, shuttle effect is not so serious, as shown in Figure 3b at C/2. This can be explained by the diffusion of polysulfides to lithium anode is slower than the total electrochemical reaction time[10, 34].

Figure 2c and Figure 2d shows the extended cycling performance and coulombic efficiency of the HE and LE Li-S cells. For the HE Li-S cell (Figure 2c), a reversible specific capacity remains at 720 mAh g^{-1}_{sulfur} after 40 cycles at C/5 rate. The coulombic efficiency at the first few cycles is less than 100%, and yet, larger than 96%. The formation of surface passivating film is believed to play an important role causing the low efficiency. Lithium metal is thermodynamically unstable in organic electrolytes and reduction of the LiTFSI salt and the DOL/DME organic solvent occurs once the lithium metal is exposed to the electrolyte[35-37]. During the first few cycles, a dynamically stable passivated film was formed, which required excess lithium to compensate the lithium loss, thus resulting in lowering the coulombic efficiency[23]. In addition, it is noticeable that the HE Li-S cell exhibiting excellent charge-discharge coulombic efficiency up to 100% after the first few cycles. This provides a convincing proof to conclude that migration of the soluble lithium polysulfide has been prevented by the LAGP, thus resulting in a decrease in the loss of active materials. The capacity fading could be attributed to the progressive formation of Li_2S, the poorly reversible discharge product, which is also the reason for the over 100% coulombic efficiency in subsequent cycles[16]. While for the LE Li-S cell (Figure 2d), poor cycling performance and extremely low coulombic efficiency are presented because of the severe shuttle effect. The coulombic efficiency later increases gradually to 80%, which may be attributed to the formation of a relative stable solid electrolyte interphase during the cell cycling.

The cells were disassembled in the argon-filled glove box after the 10th charge cycle. The morphology change of sulfur cathode and lithium anode were investigated by SEM shown in Figure 3. It is obvious that the surface of sulfur cathode cycled in LE Li-S

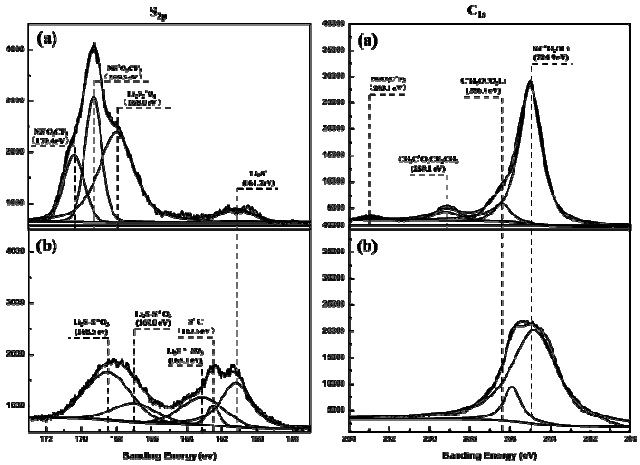

Figure 4. XPS spectra from lithium anode (a) cycled in SE Li-S cell (b) cycled in LE Li-S cell at end of 10th charge cycle.

cell shows a higher degree of roughness and breakage while the one cycled in HE Li-S cell still maintains its integrity. The dissolution of polysulfides into the liquid electrolyte and loss of active mass in the cathode composite is responsible for the structural failure of the cathode[12]. In the LE Li-S cell, the soluble polysulfides diffused through the polypropylene microporous membrane and reduced by the lithium metal, and the consecutive reaction between polysulfides and metallic lithium resulting in severe corrosion of lithium anode as shown in Figure 3f. While in the HE Li-S cell, the dissolved polysulfides were blocked on the cathode side by the LAGP solid electrolyte and the metallic lithium would never have chance to get react with the polysulfides. As a comprehensive model of dendrite growth asserts, lithium plating is faster on protrusions of electrodes.[38] The excellent mechanical strength of the LAGP is sufficient to prevent Li metal dendrite initiation and the growth of lithium dendrites is suppressed successfully. By employing the solid electrolyte, corrosion of the lithium anode is completely avoided and the growing of lithium dendrites is also absolutely suppressed by the mechanical strength. Therefore, the uniformity of lithium deposition/dissolution during repeated charge-discharge process was ensured and a relatively dense surface as smooth as the fresh lithium metal was still maintained (Figure 3e).

XPS analysis was used to further prove whether there was any side reaction between metallic lithium and the polysulfides in the HE Li-S cell or not. Figure 4 and Figure 2S show S_{2p}, C_{1s}, F_{1s} and O_{1s} spectra of lithium anode surfaces after cycled in HE and LE Li-S cells. Broad peaks were deconvoluted to specific peaks in order to identify the various element oxidation states present in the sample surface. For the S_{2p} and the C_{1s} spectra measured from lithium anode cycled in the HE cell, the peaks are attributed to products of TFSI anion and electrolyte solvents reduction, such as Li_2S (161.2 eV), $Li_2S_2O_4$ (168.0 eV, 293.1 eV), -NSO_2CF_3 (169.3 eV, 170.4 eV, 293.1 eV), RCH_2OLi (284.9 eV), CH_3OCO_2Li (286.4 eV), $CH_3CO_2CH_2CH_3$ (289.1 eV) [14, 33, 39-41]. These various possible surface species can also support the following reaction schemes as the reduction of LiTFSI in electrolyte proposed by Aurbach et al. [14, 39]

$LiN(SO_2CF_3)_2 + ne^- + nLi^+ \rightarrow Li_3N + Li_2S_2O_4 + LiF + C_2F_xLi_y$

$LiN(SO_2CF_3)_2 + 2e^- + 2Li^+ \rightarrow Li_2NCF_3SO_2 + LiF + CF_3SO_2Li$

$Li_2S_2O_4 + 6e^- + 6Li^+ \rightarrow 2Li_2S + 4Li_2O$

$Li_2S_2O_4 + 4e^- + 4Li^+ \rightarrow Li_2SO_3 + Li_2S + Li_2O$

The peak at 161.2 eV (identified as Li_2S) appeared in the S_{2p} spectra of the two metallic lithium samples. Li_2S existed on the surface of lithium anode cycled in the LE cell was mainly from the reaction between lithium anode and high-order polysulfides that migrated from the sulfur cathode. While in the HE Li-S cell, polysulfides were blocked by the LAGP solid electrolyte, Li_2S existed on the surface of cycled lithium anode derived from the decomposition of LiTFSI. Therefore, peak intensity of the Li_2S in the lithium anode cycled in the LE Li-S cell is much stronger than the one in the HE Li-S cell as shown in Figure 4. In addition, of the two samples, deconvolution of the broad S_{2p} peaks around 165-172 eV to different sharper peaks at 170.4, 169.3, 168.0 and 168.5, 167.0 eV, these variety of oxidation states of the sulfur-containing species formed on lithium reflect the degree of LiTFSI decomposition which is a key factor to the source of Li_xSO_y species in LiTFSI system[41]. In the LE Li-S cell system, decomposition of LiTFSI on lithium electrode can be prevented by reduced products of polysulfides[33]. Due to the presence of the polysulfides in the LiTFSI system, LiTFSI in the LE Li-S cell was decomposed less than in the HE Li-S cell where polysulfides were limited on the cathode side.

Figure S3 displays the EDS spectra collected from the surfaces of the cycled LAGP solid electrolyte. The spectrum of the LAGP surface close to the anode side shows that no sulfur appears (Figure S3a), while sulfur detected to be present on the surface next to the cathode side which probably derives from irreversible Li_2S progressively formed on that surface during cycling (Figure S3b). An another convincing evidence that no sulfur is observed on the on the LAGP surface close to the lithium anode side further demonstrates that soluble polysulfides are perfectly blocked by the LAGP solid electrolyte. In another word, the typical shuttle effect in common Li-S batteries is successfully eliminated by the LAGP solid electrolyte.

Experimental

Stoichiometric amounts of lithium carbonate Li_2CO_3(A.R.), alumina Al_2O_3(A.R.), germanium oxide GeO_2 (99.99%), and ammonium dihydrogen phosphate $(NH_4)H_2PO_4$ (A.R.) were used as starting materials to prepare the $Li_{1.5}Al_{0.5}Ge_{1.5}(PO_4)_3$ solid electrolyte (SE) by the conventional high temperature solid-state-reaction method[42, 43]. A planetary ball mill was used to thoroughly mixed the starting materials and heated at 700°C in an alumina crucible for 4 h to decompose Li_2CO_3 and $(NH_4)H_2PO_4$. The precursors were reground and heated at 800°C for 6h to obtain SE powder. The SE powder was then pressed into thick pellets and sintered at 900°C for 12 h. All of the above heat treatments were carried out in the air atmosphere. The density of the obtained circular SE pellet (diameter 17.5 mm and thickness 0.65 mm) was about 3.2 gcm^{-3}. For the total lithium ion conductivity measurement of the pellet, gold films were sputtered onto the both sides of the sample and the measured value is about 1.77×10^{-4} S cm^{-1}.

KB/S composite was first prepared by heating the ground mixture of KB and S at 155°C for 12 h under vacuum, with 60 wt% sulfur loading in the composite. Then the sulfur electrodes were prepared by doctor blade casting a mixture containing 80 wt% KB/S composite, 10 wt% acetylene black, 5 wt% Carboxy

Methylated Cellulose and 5wt% Styrene Butadiene Rubber binder onto Al current collector foil. The electrodes were cut into sheets with 12 mm in diameter and dried at 60°C for 12 h under vacuum.

The batteries were tested by galvanostatic cycling in the voltage range of 1.0-3.0 V vs Li/Li^+ on a LAND CT2001A battery test system (Wuhan, China). Specific capacities were calculated based on sulfur mass. Electrochemical impedance measurements of the cell were performed on a Autolab PGSTAT302N Electrochemical Workstation (ECO CHEMIE B.V, Netherlands) by a Frequency Response Analyzer (FRA) and a small perturbation voltage of 10 mV in the frequency range from 1 MHz to 100 mHz was applied. All electrochemical tests were conducted at room temperature.

Cycled cells were disassembled in an argon-filled glove box. Lithium metal foils, LAGP, and sulfur electrodes were rinsed several times with pure DME and further dried for 6h in the argon-filled glove box. They were all placed in an inert atmosphere during sample preparation and transferring into the tested instruments. Morphology changes of the KB/S cathode film and lithium metal foil were carried out with a HITACHI S-3400 scanning electron microscope (SEM). The elemental mapping results were examined with an energy dispersive spectrometer (EDS) attached to the HITACHI SEM. The elements at the surface of the cycled lithium metal foil were observed by a Thermo scientific ESCALAB 250 X-ray photoelectron spectroscopy (XPS) and monochromatic $Al_{k\alpha}$ as the X-ray source. Binding energy scale was calibrated by C_{1s} peak, corresponding to hydrocarbon adsorbed on the sample surface (285.0 eV). The spectra were analyzed and deconvoluted using the Version 4.1 software (XPSPEAK). The Shirley background, the mixed Gaussian-Lorentzian approach, was used for the fitting of the high resolution S_{2p} ,C_{1s}, F_{1s} and O_{1s} peaks.

Conclusions

A novel type room temperature lithium sulfur cell based on hybrid electrolyte was successfully constructed. The inorganic solid electrolyte LAGP was employed both as the lithium ion conductor and the separator to block the soluble polysulfides. With an open circuit voltage of about 3 V, the cells were successfully discharged and charged for dozens of cycles with an excellent coulombic efficiency of 100%. The hybrid cell exhibited initial discharge specific capacities of up to 1528 mAh g^{-1}, 1386 mAh g^{-1} and 1341 mAh g^{-1}, respectively, at C/20, C/5 and C/2 rates. Reversible specific capacity remains at 720 $mAhg^{-1}$ after 40 cycles at C/5 rate. XPS and EDS spectra demonstrated that there was no side reaction between the lithium metal and the polysulfides in the hybrid electrolyte based lithium sulfur cell. As a results, the shuttle effect can be completed eliminated by employing the hybrid electrolyte.

Acknowledgements

This work was financially supported by the National Science Foundation of China (NFSC) project No. 51372263 and No. 51201177; opening project of CAS Key Laboratory of Materials for Energy Conversion. Prof. B. V. R. Chowdari (Department of Physics, National University of Singapore) is highly acknowledged for helpful discussions.

Notes and references

[a] *CAS Key Laboratory of Materials for Energy Conversion, Shanghai Institute of Ceramics, Chinese Academy of Sciences, Shanghai 200050, P. R.China. Fax: +86-21-52413903; Tel: +86-21-52411704; E-mail: zywen@mail.sic.ac.cn*

† Electronic Supplementary Information (ESI) available. See DOI: 10.1039/b000000x/

1. P. G. Bruce, S. A. Freunberger, L. J. Hardwick and J. M. Tarascon, *Nat Mater*, 2012, **11**, 19-29.
2. A. Manthiram, Y. Fu and Y. S. Su, *Accounts of chemical research*, 2012.
3. X. L. Ji, K. T. Lee and L. F. Nazar, *Nat Mater*, 2009, **8**, 500-506.
4. L. W. Ji, M. M. Rao, H. M. Zheng, L. Zhang, Y. C. Li, W. H. Duan, J. H. Guo, E. J. Cairns and Y. G. Zhang, *J Am Chem Soc*, 2011, **133**, 18522-18525.
5. Y. Fu, Y. S. Su and A. Manthiram, *Angew Chem Int Ed Engl*, 2013, **52**, 6930-6935.
6. T. Lin, Y. Tang, Y. Wang, H. Bi, Z. Liu, F. Huang, X. Xie and M. Jiang, *Energ Environ Sci*, 2013, **6**, 1283.
7. S. Zheng, Y. Chen, Y. Xu, F. Yi, Y. Zhu, Y. Liu, J. Yang and C. Wang, *Acs Nano*, 2013, **7**, 10995-11003.
8. T. G. Jeong, Y. H. Moon, H. H. Chun, H. S. Kim, B. W. Cho and Y. T. Kim, *Chem Commun (Camb)*, 2013.
9. S. Zheng, Y. Wen, Y. Zhu, Z. Han, J. Wang, J. Yang and C. Wang, *Adv Energy Mater*, 2014, n/a-n/a.
10. Y. V. Mikhaylik and J. R. Akridge, *J Electrochem Soc*, 2004, **151**, A1969-A1976.
11. D. Bresser, S. Passerini and B. Scrosati, *Chem Commun (Camb)*, 2013, **49**, 10545-10562.
12. X. L. Ji and L. F. Nazar, *J Mater Chem*, 2010, **20**, 9821-9826.
13. Y.-X. Yin, S. Xin, Y.-G. Guo and L.-J. Wan, *Angewandte Chemie International Edition*, 2013, n/a-n/a.
14. D. Aurbach, E. Pollak, R. Elazari, G. Salitra, C. S. Kelley and J. Affinito, *J Electrochem Soc*, 2009, **156**, A694-A702.
15. X. Liang, Z. Wen, Y. Liu, M. Wu, J. Jin, H. Zhang and X. Wu, *J Power Sources*, 2011, **196**, 9839-9843.
16. S. S. Zhang, *J Electrochem Soc*, 2012, **159**, A920-A923.
17. S. S. Zhang, *Electrochim Acta*, 2012, **70**, 344-348.
18. M. K. Song, Y. G. Zhang and E. J. Cairns, *Nano Lett*, 2013, **13**, 5891-5899.
19. S. S. Zhang and J. A. Read, *J Power Sources*, 2012, **200**, 77-82.
20. S. Z. Xiong, K. Xie, Y. Diao and X. B. Hong, *Electrochim Acta*, 2012, **83**, 78-86.
21. S. S. Zhang, *J Power Sources*, 2013, **231**, 153-162.
22. K. Takada, *Acta Mater*, 2013, **61**, 759-770.
23. W. Xu, J. L. Wang, F. Ding, X. L. Chen, E. Nasybutin, Y. H. Zhang and J. G. Zhang, *Energ Environ Sci*, 2014, **7**, 513-537.
24. M. Nagao, Y. Imade, H. Narisawa, T. Kobayashi, R. Watanabe, T. Yokoi, T. Tatsumi and R. Kanno, *J Power Sources*, 2013, **222**, 237-242.
25. M. Agostini, Y. Aihara, T. Yamada, B. Scrosati and J. Hassoun, *Solid State Ionics*, 2013, **244**, 48-51.
26. M. Hagen, S. Dorfler, H. Althues, J. Tubke, M. J. Hoffmann, S. Kaskel and K. Pinkwart, *J Power Sources*, 2012, **213**, 239-248.
27. X. Xu, Z. Wen, X. Wu, X. Yang and Z. Gu, *Journal of the American Ceramic Society*, 2007, **90**, 2802-2806.
28. Z. F. Deng, Z. A. Zhang, Y. Q. Lai, J. Liu, J. Li and Y. X. Liu, *J Electrochem Soc*, 2013, **160**, A553-A558.
29. N. Jayaprakash, J. Shen, S. S. Moganty, A. Corona and L. A. Archer, *Angew Chem Int Ed Engl*, 2011, **50**, 5904-5908.
30. Y. S. Su and A. Manthiram, *Nat Commun*, 2012, **3**, 1166.
31. R. Elazari, G. Salitra, A. Garsuch, A. Panchenko and D. Aurbach, *Adv Mater*, 2011, **23**, 5641-5644.
32. K. Kumaresan, Y. Mikhaylik and R. E. White, *J Electrochem Soc*, 2008, **155**, A576.

33. S. Xiong, K. Xie, Y. Diao and X. Hong, *J Power Sources*, 2013, **236**, 181-187.
34. J. Brückner, S. Thieme, H. T. Grossmann, S. Dörfler, H. Althues and S. Kaskel, *J Power Sources*, 2014, **268**, 82-87.
35. D. Aurbach, I. Weissman, A. Zaban and O. Chusid, *Electrochim Acta*, 1994, **39**, 51-71.
36. D. Aurbach, O. Youngman, Y. Gofer and A. Meitav, *Electrochim Acta*, 1990, **35**, 625-638.
37. D. Aurbach, A. Zaban, Y. Gofer, Y. E. Ely, I. Weissman, O. Chusid and O. Abramson, *J Power Sources*, 1995, **54**, 76-84.
38. C. Monroe and J. Newman, *J Electrochem Soc*, 2003, **150**, A1377.
39. D. Aurbach, A. Zaban, Y. Ein-Eli, I. Weissman, O. Chusid, B. Markovsky, M. Levi, E. Levi, A. Schechter and E. Granot, *J Power Sources*, 1997, **68**, 91-98.
40. H. Ota, Y. Sakata, X. Wang, J. Sasahara and E. Yasukawa, *J Electrochem Soc*, 2004, **151**, A437.
41. Y. Diao, K. Xie, S. Z. Xiong and X. B. Hong, *J Electrochem Soc*, 2012, **159**, A1816-A1821.
42. C. J. Leo, G. V. S. Rao and B. V. R. Chowdari, *Solid State Ionics*, 2003, **159**, 357-367.
43. H. Kitaura and H. Zhou, *Energ Environ Sci*, 2012, **5**, 9077.